

THE E895 π^- CORRELATION ANALYSIS – A STATUS REPORT

M.A. Lisa^j, for the E895 Collaboration*

N.N. Ajitanand^m, J. Alexander^m, D. Best^a, P. Brady^e, T. Case^a,
 B. Caskey^e, D. Cebra^e, J. Chance^e, I. Chemakin^d, P. Chung^m,
 V. Ciancioloⁱ, B. Cole^d, K. Crowe^a, A. Das^j, J. Draper^e, S. Gushue^b,
 M. Gilkes^l, M. Heffner^e, H. Hiejima^d, A. Hirsch^l, E. Hjort^l, L. Huo^g,
 M. Justice^h, M. Kaplan^c, D. Keane^h, J. Kintner^f, D. Krofcheck^k,
 R. Lacey^m, J. Lauret^m, E. LeBras^m, H. Liu^h, Y. Liu^g, R. McGrath^m,
 Z. Milosevich^c, D. Olson^a, S. Panitkin^h, C. Pinkenburg^m, N. Porile^l,
 G. Rai^a, H.-G. Ritter^a, J. Romero^e, R. Scharenburg^l, L. Schroeder^a,
 R. Soltzⁱ, B. Srivastava^l, N.T.B. Stone^b, T.J. Symons^a, S. Wang^h,
 R. Wells^j, J. Whitfield^c, T. Wienold^a, R. Witt^h, L. Wood^e, X. Yang^d,
 W. Zhang^g, Y. Zhang^d

^aLBL, ^bBNL, ^cCMU, ^dColumbia, ^eUC Davis, ^fSt. Mary's College,

^gHarbin Institute, China, ^hKent State, ⁱLLNL, ^jOhio State,

^kAuckland, NZ, ^lPurdue, ^mSUNY at Stony Brook

INTRODUCTION– E895 MOTIVATION AND EXPERIMENT

A primary goal of high-energy heavy ion physics is to create and study the quark-gluon plasma (QGP), a phase of matter in which partonic– instead of hadronic– degrees of freedom describe the system. Several transport, hydrodynamic, and nucleation theories^{1, 2, 3, 4} suggest that energy densities achieved in central collisions between heavy ions at AGS energies may be sufficient to create the QGP.

If the QGP is created in a heavy ion collision, the timescale for particle emission is expected to be longer than a scenario in which only ordinary hadronic degrees of freedom play a role^{5, 6}, due to the extra time of hadronization. Thus, one proposed signature for QGP formation has been a large apparent source lifetime as measured by pion HBT measurements. However, HBT analyses of very heavy ion collisions at the maximum AGS energy^{7, 8} (10.6 AGeV) and at CERN SPS^{9, 10} (158 AGeV) do not indicate emission timescales longer than that expected from normal hadronic physics. Thus, it may seem pointless to look for long lifetimes at energies *below* maximum AGS energy.

However, recent hydrodynamical calculations by Rischke and collaborators suggest that some signatures of QGP creation– including large source lifetimes from HBT– may *only* be apparent very close to the threshold of QGP formation⁶. The QGP threshold energy corresponds to a “softest point” in the Equation of State^{6, 11, 12}. For a source created at this energy, the lifetime is longer because the system does not expand and

*Presented at the 14th Winter Workshop on Nuclear Dynamics, Snowbird, UT, Feb 1998

cool as rapidly as it would if there were no phase transition. For collisions at energies much above this threshold energy, the system (which is in the QGP phase) expands and cools rapidly, and the lifetime effect is diminished.

The value of the threshold energy, then, is of paramount importance. One would like to study collisions around this energy, to better recognize and understand the transition. Since this value is not known in principle, it is important to perform systematic studies of nuclear collisions as a function of energy.

Further motivation to look for QGP turn-on at the AGS comes from recent thermochemical meta-analyses¹³ of experimental spectra and yields from collisions at maximum AGS and SPS energies. Based on an equilibrium scenario, these analyses suggest that already at the maximum AGS energy, the system freezes out on the border between QGP and normal nuclear matter. This would imply that the system had cooled from a hotter, denser state in the QGP phase. Similar analyses in the SIS/Bevalac energy region¹⁴ (0.1-1.0 AGeV) place the systems created at these energies solidly in the realm of normal hadronic matter, but smoothly approaching the hadronic-matter/QGP “border” (in the phase diagram) as the bombarding energy increases.

Using the Time Projection Chamber^{15, 16} used in the EOS experiments at the Bevalac, the E895 collaboration has measured roughly 0.5-1 million collision events at 2, 4, 6, and 8 AGeV at the Brookhaven AGS. The results presented here represent a small ($\sim 2\%$) fraction of the total available statistics.

The TPC was located in the MPS magnet operated with a field of 0.75 or 1 T. The active volume of the TPC is a rectangular region 154 cm x 96 cm x 75 cm in the beam, bend, and drift directions, respectively. Electrons liberated by charged particles passing through the TPC drift to 15360 pads arranged in 128 rows at the bottom of the TPC. The signal on each pad is sampled and digitized every 100 ns (140 time buckets), providing roughly 2 million 3-dimensional pixels in which the ionization is measured. “Hits” are reconstructed from the pixels, corresponding to a track crossing a padrow. Tracks are then formed from the found hits, giving continuous tracking and particle identification with nearly 4π acceptance in the center of mass.

HBT ANALYSIS AND THE NEED FOR PAIR-WISE CUTS

The correlation function $C(\vec{k}_1, \vec{k}_2)$ is given by constructing the ratio

$$C(\vec{k}_1, \vec{k}_2) = \frac{R(\vec{k}_1, \vec{k}_2)}{B(\vec{k}_1, \vec{k}_2)} \quad (1)$$

where \vec{k}_1 and \vec{k}_2 are the momenta of the two particles (here, pions) in a pair. R is the measured (“real”) 2-particle yield. The background yield B should contain all phase space and single-particle detector acceptance effects. It is constructed via the event-mixing technique; we mix π^- from a given event with pions from the previous 15 events.

In one-dimensional HBT analyses, such as the one discussed here, the real and background distributions are binned in Q_{inv} , where $Q_{inv}^2 = (\vec{k}_1 - \vec{k}_2)^2 - (E_1 - E_2)^2$. $C(Q_{inv})$ is normalized to unity at large Q_{inv} . All correlation functions presented here are binned in Q_{inv} in GeV/c.

Three distinct “levels” of cuts are applied to the data input to the HBT analysis. Firstly, event-wise cuts are applied, to select a range of charged particle multiplicity, and a range of primary vertex positions (the latter helps eliminate events from upstream of the target). In the current analysis, the multiplicity range for the 2 and 4 AGeV events

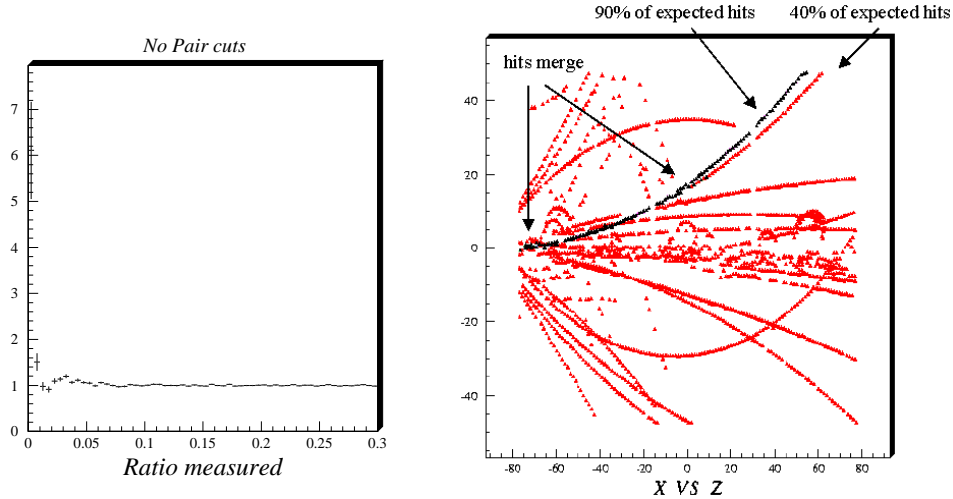


Figure 1. **Left** The correlation function with only event-wise and track-wise cuts applied. Structure at low Q_{inv} is due primarily to track-splitting and merging. **Right** Hits for true low- Q_{inv} pair in a very low multiplicity event. Hits close to the primary vertex merge, and are assigned to one of the tracks.

selected was large (50-200 and 50-250, respectively, corresponding to a maximum impact parameter of about 8 fm), while the 8 AGeV data was more central (multiplicity \approx 200-300, or $b \approx$ 0-3 fm).

Secondly, track-wise cuts are performed. These include selection of particle type, goodness of the track fit, track length, and phase space (\vec{k}) cuts. In most E895 analyses, the most crucial track quality cut has been on how well the track projects back to the primary vertex. These cuts are applied to events and particles both in the measured yield R as well as the background B .

Below, we discuss the need for a third level of cuts— pair-wise cuts— to reduce two-particle acceptance effects.

Split tracks

Using only track-wise cuts to select “good” pions, the measured correlation function for the 4 AGeV data is shown in the left panel of Figure 1. Simulations and visual inspection of individual events indicate that the strong and unrealistic structure seen at low Q_{inv} is a result of track splitting. Here, a track which crosses, say, 80 padrows (and so in principle should produce 80 “hits” (see above)), is broken by the pattern recognition software into two tracks with 20 and 35 hits. (Overall loss of 30% of the hits on a track— even those not split— is typical, due to the high track density and hit merging.) Naturally, the reconstructed momentum difference for this false pair is low. Such pairs will be seen in the “real” distribution R , but not in the background B . Track splitting mainly affects the lowest Q_{inv} bin, but the effect extends to \sim 30 MeV/c.

A possible track-wise cut that can remove this effect would be to require that more than 50% of a track be reconstructed. The problem with this approach is seen in the right panel of Figure 1. A large fraction of “true” low- Q_{inv} pairs are eliminated as well, since, close to the primary vertex, the tracks are closer than the two-hit resolving distance (\sim 1.5 cm), so only one hit is found; this hit is assigned to one of the tracks.

The solution implemented is to require that the *sum* of the reconstructed fraction of the pair is greater than 100%. This removes split tracks, while preserving true low- Q_{inv} pairs. The correlation function with this cut is shown in the upper left panel of Figure 2.

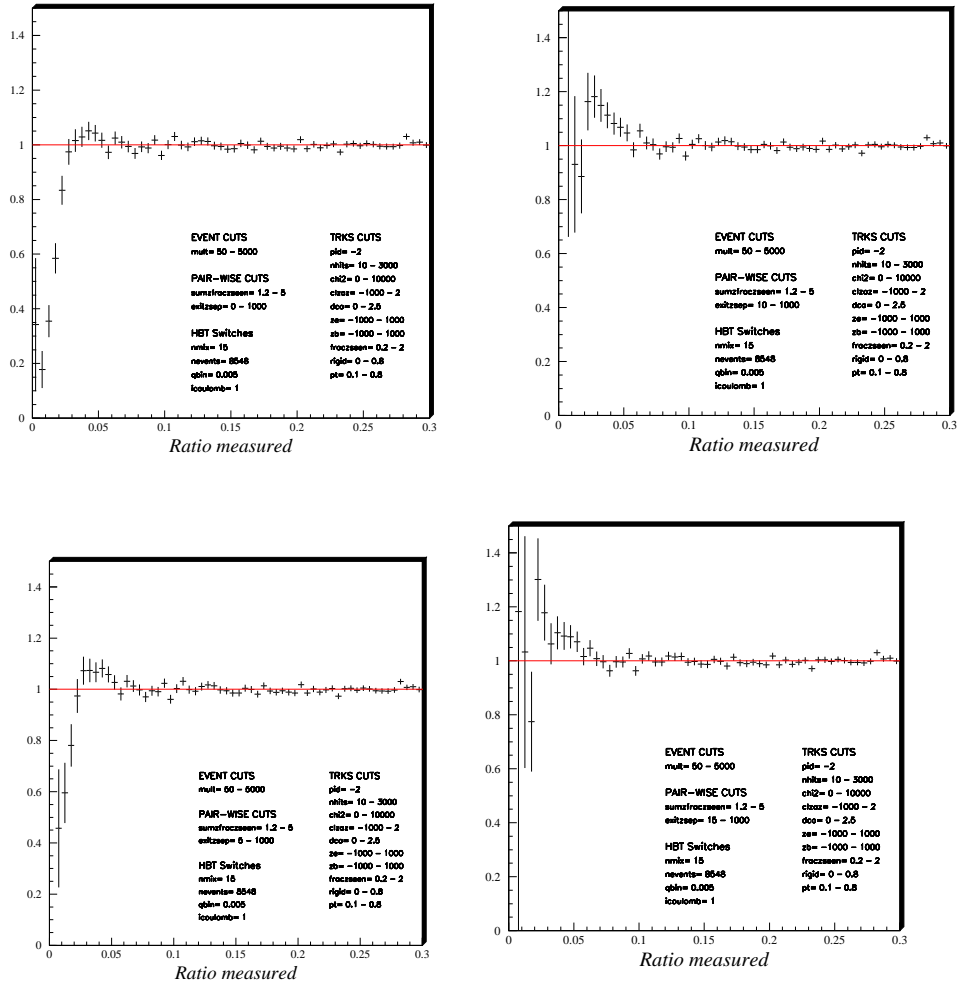


Figure 2. After splitting is removed, the correlation function is plotted (for the 4 AGeV data) for a cut on exit separation of 0 cm (top left), 5 cm (bottom left) 10 cm (top right) and 15 cm (bottom right).

Merged Tracks

The large hole at low Q_{inv} in the top left panel of Figure 2 is due to track merging—the situation in the right panel of Figure 1 taken to the extreme. Merging affects pairs in the real distribution, but not in the background. Since the merged tracks (affecting the real distribution R) cannot be recovered, the goal is to remove pairs from the background distribution B which *would* merge if the pions came from the same event.

To this end, we cut on the distance between the projected points at which the two tracks exit the TPC. For the E895 geometry, cutting on the distance between exit points is superior to, say, cutting on the distance between the tracks at some fixed plane (as is appropriate for a different detector geometry⁷), since the tracks can exit through any of the six sides of the rectangular detector. A close pair that is separated by 2 cm at an intermediate plane would be resolvable if the pions were to pass through 40 more padrows later on, while it would be unresolvable if they exited the TPC just after the cut plane.

As seen in Figure 2, raising the exit separation cut from 0 to 10 cm reduces the low- Q_{inv} hole, while further increases only reduce statistics.

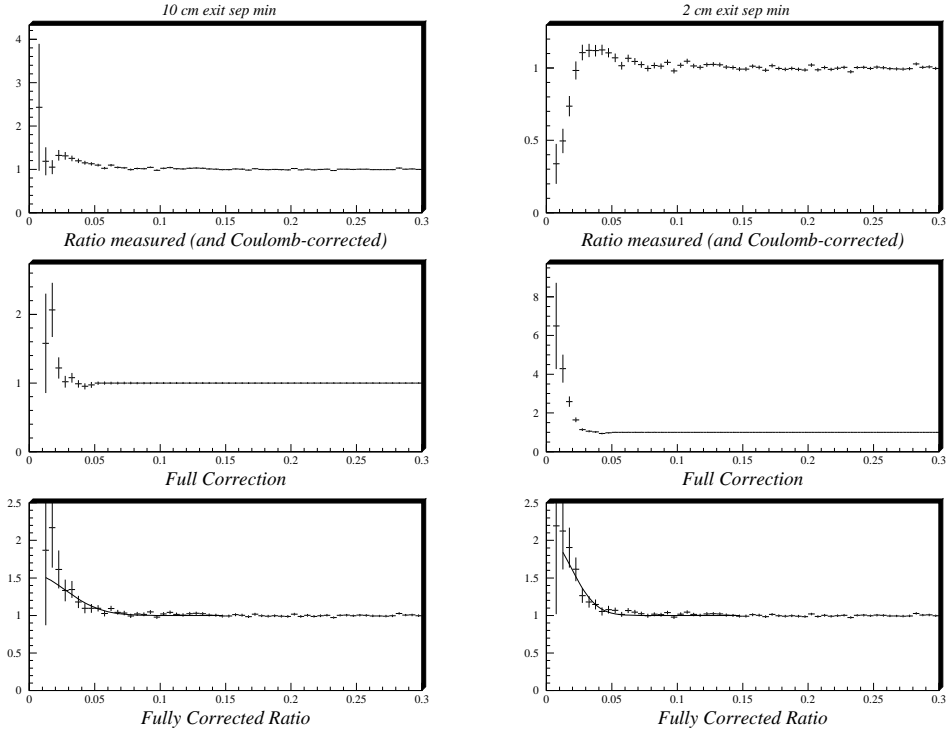


Figure 3. Correlation functions for a 10 cm (left) and 2 cm exit separation cut (right) from the 4 AGeV data. Top panels show the correlation only corrected by the Gamow function. Middle panels show the 2-track acceptance correction discussed in the text. Bottom panels show the preliminary corrected correlation functions.

CORRECTIONS APPLIED TO THE CORRELATION FUNCTION

Coulomb Correction

To measure the pure Bose-Einstein correlation, it is common practice to “correct” for the Coulomb repulsion between the charged pions when constructing the correlation function. We apply this pair-wise correction G to the pairs in the background, so the measured correlation becomes

$$C(\vec{k}_1, \vec{k}_2) = \frac{R(\vec{k}_1, \vec{k}_2)}{B(\vec{k}_1, \vec{k}_2) \times G(\vec{k}_1, \vec{k}_2)} \quad (2)$$

In the present analysis, we use the standard Gamow function¹⁷ for G . The Gamow function is known to over-estimate the Coulomb correction for large source sizes¹⁸. The more correct Coulomb correction obtained by integrating the Coulomb wavefunction is expected to change fit parameters by $\sim 10\%$ ^{7, 18}, as compared to fits using the Gamow correction. However, presentation of results with the Gamow correction are useful for comparison to other correlation analyses, which often use this correction.

With all cuts and Gamow correction applied, the correlation function for the 4 AGeV data is shown in the top left panel of Figure 3.

Simulations and Acceptance Correction

Even with the pair-wise cuts, detailed simulations show that two-track acceptance effects persist; these include some residual track splitting and merging. However the larger effect on the correlation function is the finite resolution and distortion of the relative momentum. For example, for some set of cuts, Figure 4 shows the relative

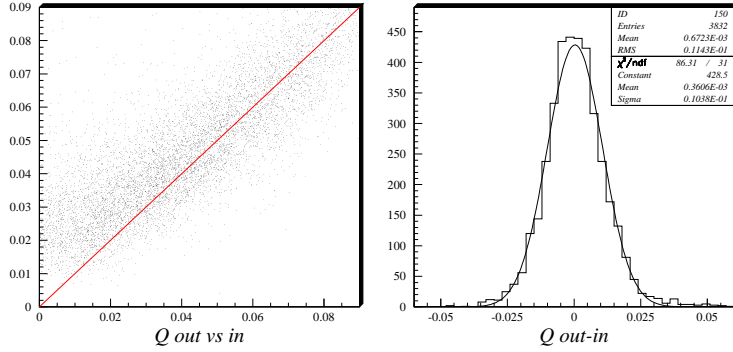


Figure 4. Simulation results for low- Q_{inv} pairs. **Left:** For very low relative momenta, the reconstructed Q_{inv} is distorted due to phase space. **Right:** Above $Q_{inv}=40$ MeV/c, the relative momentum is resolved with a resolution of ~ 10 MeV/c.

momentum resolution for simulated pairs of pions. Above $Q_{inv} \sim 40$ MeV/c, the reconstructed Q_{inv} tracks with the input Q_{inv} , with a resolution of about 10 MeV/c. For very low Q_{inv} , the relative momentum is distorted due to phase space and 2-track efficiency effects. These simulations include multiple scattering in the detector entrance window, as well as in the gas. The simulation is done at the pixel level, and the full pattern recognition and reconstruction code is run.

The magnitude and character of these effects depend strongly on (1) \vec{k}_1 and \vec{k}_2 (in six dimensions!) themselves, due to the irregular geometry of the TPC, and (2) the particular track-wise and pair-wise cuts used in a given analysis. Rather than attempting to parametrize these effects as a function of this huge number of variables, we employ detailed simulations directly in our HBT analysis. The technique described here follows closely that of the NA44 collaboration¹⁹.

The singles momentum distribution (for some impact parameter cut) is fit with a thermal source distribution. This distribution is then sampled to give pion pairs at low- Q_{inv} , which are then embedded at the pixel level into real data events. This method ensures that the true noise distribution and track density present in the data affects the reconstruction of simulated particles in the same way as it does the measured particles. It also ensures that the same (\vec{k}_1, \vec{k}_2) distribution is used in the corrections as in the data analysis. For each pair input to the simulation, there are two input momenta (\vec{k}_1, \vec{k}_2) , and n output (reconstructed) momenta $(\vec{k}'_1, \vec{k}'_2, \dots, \vec{k}'_n)$. An ideal detector and event reconstruction would yield $n = 2$ and $\vec{k}'_i = \vec{k}_i$. The purpose of the correction is to remove effects of the deviation from this idealization. It should be noted that effects of track merging and splitting ($n \neq 2$) and momentum resolution ($\vec{k}'_i \neq \vec{k}_i$) will depend on the cuts we use. Thus, we would require our correction to track with any changes in cut values.

The acceptance correction is then defined as

$$K = \frac{C(\text{ideal})}{C(\text{reconstructed})} = \frac{R(\vec{k}_1, \vec{k}_2)}{B(\vec{k}_1, \vec{k}_2)} \frac{R(\vec{k}'_1, \vec{k}'_2)}{B(\vec{k}'_1, \vec{k}'_2)} \quad (3)$$

where $R(\vec{k}_1, \vec{k}_2)$ is the real distribution of simulated (input) pairs weighted by the correlation function:

$$R(\vec{k}_1, \vec{k}_2) = \frac{d^6 N}{d^3 \vec{k}_1 d^3 \vec{k}_2} \times C(\vec{k}_1, \vec{k}_2) \quad (4)$$

and $B(\vec{k}_1, \vec{k}_2)$ is the background distribution

$$B(\vec{k}_1, \vec{k}_2) = \frac{d^6 N}{d^3 \vec{k}_1 d^3 \vec{k}_2} \quad (5)$$

Note that use of these relations to construct the numerator in equation 3 (as opposed to simply using $C(\vec{k}_1, \vec{k}_2)$), allows an accounting for the statistical error. In forming the ideal correlation function, the only cuts applied to the input tracks are phase-space cuts (rapidity and p_T)—no track quality cuts.

The denominator of equation 3 is formed with the reconstructed particles, with momenta \vec{k}'_i . As mentioned above, the number n of these particles for one input pair, will depend on the particular value of track-wise and pair-wise cuts used. In forming this reconstructed correlation function, the same cuts are applied as to the measured data.

$R(\vec{k}'_1, \vec{k}'_2)$ is formed by binning the distribution according to the reconstructed momenta \vec{k}'_i , but *weighted* by the *true* Bose-Einstein correlation function, which is a function of the input (“true”) momenta \vec{k}_i .

$$R(\vec{k}'_1, \vec{k}'_2) = \frac{d^6 N}{d^3 \vec{k}'_1 d^3 \vec{k}'_2} \times C(\vec{k}_1, \vec{k}_2) \quad (6)$$

In the simulation, then, we must keep track of which input particle (\vec{k}_i) gives rise to a reconstructed track (\vec{k}'_i).

Correction to the Coulomb Correction

To complete the acceptance correction (Equation 3), we must calculate the background distribution of reconstructed particles. In doing so, however, we account for the fact that the Coulomb correction G applied to the measured background distribution (Equation 2) is calculated using the measured Q_{inv} , and not the true Q_{inv} ^{19, 7}. We account for this finite resolution effect by constructing the reconstructed background as

$$B(\vec{k}'_1, \vec{k}'_2) = \frac{d^6 N}{d^3 \vec{k}'_1 d^3 \vec{k}'_2} \times \frac{G(\vec{k}_1, \vec{k}_2)}{G(\vec{k}'_1, \vec{k}'_2)} \quad (7)$$

where G is the Coulomb correction (here, just the Gamow function).

Note that these considerations make it clear that the corrections for Coulomb repulsion and detector acceptance cannot be factorized.

Notes

We see that in constructing the acceptance correction, the correlation function was used as a weight. But this is the very thing we are trying to measure! Again following the formalism of the NA44 collaboration¹⁹, we employ an iterative approach to the problem.

We assume a Gaussian source distribution $\rho(r) \sim e^{-r^2/R^2}$, which would lead to a Gaussian correlation function

$$C(Q_{inv}) = 1 + \lambda e^{-(Q_{inv} \cdot R)^2} \quad (8)$$

where λ is the so-called coherence parameter. At the first iteration, we assume some reasonable values for R and λ , and construct the correction. We then fit the corrected correlation function with the form (8). This gives new values of R and λ , which are then used as inputs for the next iteration. It is found that the fit parameters stabilize within about 4 iterations, and are robust against variations in the initial guess.

This procedure will become even more important when we use the full Coulomb wave integration (instead of Gamow), since then the Coulomb correction itself depends on the source distribution.

Finally, it may be possible to do away with the assumption of a Gaussian source altogether, by taking the Fourier transform of the correlation function to extract the source distribution²⁰ in the iterative process. We plan to try this as a next step.

RESULTS

In Figure 3 are shown the raw (but Gamow-corrected) correlation function, the acceptance correction, and the corrected correlation function for two different cuts on the exit separation for the 4 AGeV data. As noted above, the low- Q_{inv} hole in the raw correlation function, due to track merging, varies with the value of this cut. However, when the same cuts are applied to the reconstructed tracks from the simulation, the acceptance correction is seen to change as well— a larger correction is calculated, as expected, for the looser cut on exit separation. Finally, when the correction is applied, it is seen that the correlation functions for the two different cuts agree.

Variations in other cut parameters also produce different raw correlation functions, and different correction factors. However, the corrected correlation function is robust against reasonable variations. This stability gives us confidence in our ability to remove the nontrivial effects of the detector. The fully corrected correlation functions for the 4 A GeV data are shown in Figure 5. Gaussian fits to the correlation function with the form of Equation 8 give an invariant radius of $R = 5.8 \pm 0.7$ fm and incoherence parameter $\lambda = 0.83 \pm 0.25$.

The same stability is seen in the analysis of the 2 AGeV data. Figure 6 shows the corrected correlation function for two different values of the exit separation cut. Although the data points themselves fall almost on top of each other, the Gaussian fit parameters are seen to be very sensitive to small variations. These variations in the fit parameters can be treated as a systematic error. Fits, shown in the figure, give $R = 5.9 \pm 1.2$ fm and $\lambda = 0.83 \pm 0.34$.

The radius parameters extracted (often called R_{inv}) are consistent with those extracted at 10 AGeV^{7, 8}, when the Gamow Coulomb correction is used. Meanwhile the λ parameters presented here higher than the values (0.45-0.6) obtained at the higher energy. This may be expected due to the decreased role of long-lived resonances, which tend to reduce λ ²¹. However, with the statistics used in this analysis, error bars are too large to confirm a difference.

Not shown here are the results for the 8 AGeV data. For this set, the corrected correlation function was *not* stable against variations in the cuts. We are currently tracking down the source of this problem, which appears to be a tracking error when the track density gets very high.

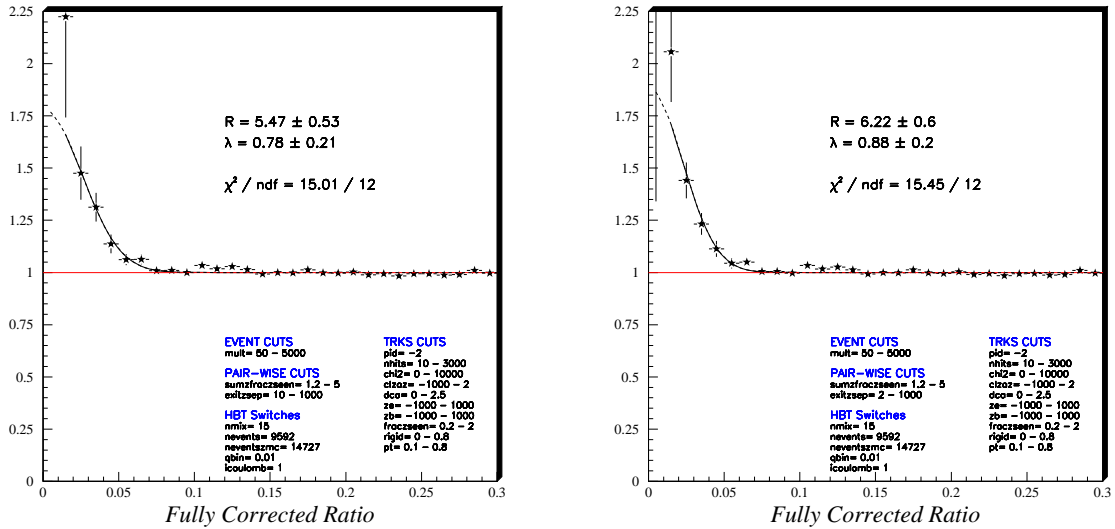


Figure 5. Preliminary fully corrected correlation functions for the 4 A GeV data are shown, for an exit separation cut of 10 cm (left) and 2 cm (right).

SUMMARY

Details of the E895 π^- correlation analysis have been presented. Along with track-wise criteria to select well constructed pions, pair-wise cuts are necessary to reduce the two-track detector acceptance effects. Remaining two-track effects can be corrected through use of detailed simulations, in which simulated low- Q_{inv} pion pairs are embedded in real data at the pixel level, and then reconstructed. The uncorrected correlations depend strongly on the cut values used, as do the corrections obtained with the simulation. However, the corrected correlation functions are largely robust against variations in the cuts.

Preliminary one-dimensional correlation functions have been presented for Au+Au collisions at 2 and 4 AGeV, with a medium-bias impact parameter distribution. Gaussian fits to these functions yield radius parameters consistent with those obtained at the maximum AGS energy, while the intercept parameter appears larger, perhaps a sign that long-lived resonances play less of a role at these energies.

A problem currently under study is that the stability of the correlations at 2 and 4 AGeV is not seen in our analysis at 8 AGeV. Resolution of this problem, greater statistics at all energies, and a multidimensional analysis will be necessary to definitively say that HBT parameters show no sharp behavior as the beam energy is changed.

ACKNOWLEDGEMENTS

The author thanks Drs. David Hardtke and Thomas Humanic for useful discussions on the acceptance correction.

This work supported by the Director, Office of Energy Research, Office of Basic Energy Sciences, Nuclear Science Division, of the U.S. Department of Energy under contract DE-AC03-76SF00098 and grants DE-FG02-89ER40531, DE-FG02-88ER40408, DE-FG02-87ER40324, by the U.S. National Science Foundation under grants PHY-9722653, PHY-9601271, PHY-9225096, and by the University of Auckland Research Committee, NZ/USA Cooperative Science Programme CSP 95/33.

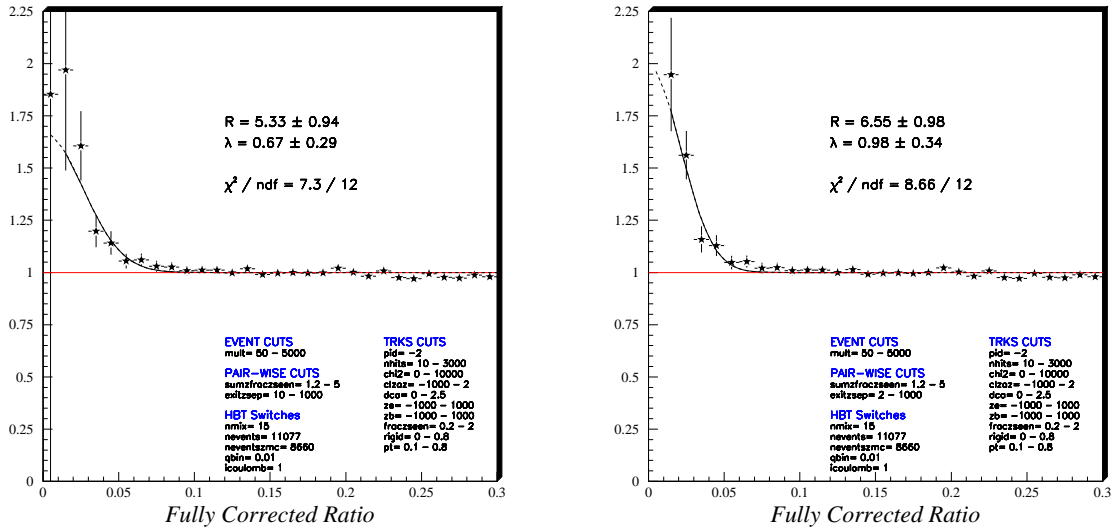


Figure 6. Preliminary fully corrected correlation functions for the 2 A GeV data are shown, for an exit separation cut of 10 cm (left) and 2 cm (right).

REFERENCES

1. B.A. Li and C.M. Ko, Nucl. Phys. **A601**, 457 (1996).
2. J.I. Kapusta, A. P. Vischer and R. Venugopalan, Phys. Rev. **C51**, 901 (1995).
3. D.H. Rischke et al., J. Phys. **G14**, 191, (1988); Phys. Rev. **D41**, 111 (1990).
4. N.K. Glendenning, Nucl. Phys. **A512**, 737 (1990).
5. S. Pratt, Phys. Rev. **C49** 2772 (1994); Phys. Rev. **D33**, 1314 (1986).
6. D.H. Rischke and M. Gyulassy, nucl-th/96039; D.H. Rischke, Nucl. Phys. **A610**, 88c (1996).
7. J. Barrette, *et al.* (E877 Collaboration), Nucl. Phys **A610**, 227c (1996); J. Barrette, *et al.*, Phys. Rev. Lett **78**, 2916 (1997).
8. M.D. Baker, *et al.* (E802 Collaboration), Nucl. Phys. **A610**, 213c (1996); B.A. Cole, *et al.* (E802 Collaboration), Nucl. Phys. **A590**, 179c (1995).
9. I.G. Bearden, *et al.* (NA44 Collaboration), Nucl. Phys. **A610**, 240c (1996).
10. K. Kadija, *et al.* (NA49 Collaboration), Nucl. Phys. **A610**, 248c (1996).
11. C.M. Hung and E.V. Shuryak, Phys. Rev. Lett. **75**, 4003 (1995).
12. D.H. Rischke, S. Bernard, J.A. Maruhn, Nucl. Phys. **A595**, 346 (1995).
13. P. Braun-Munzinger and J. Shachel, Nucl. Phys. **A606**, 320 (1996).
14. B. Hong, *et al.*, (FOPI Collaboration), “Proceedings of The International Workshop on Heavy Ion Physics at Low, Intermediate and Relativistic Energies Using 4 π Detectors,” M. Petrovici, A. Sandulescu, D. Pelte, H. Stöcker, and J. Randrup, eds. (World Scientific), p304 (1996).
15. H.G. Pugh, G. Odyniec, G. Rai, and P. Seidl, report LBL-22314 (1986).
16. G. Rai, *et al.*, IEEE Trans. Nucl. Sci. **37**, 56 (1990).
17. M. Gyulassy, S.K. Kaufmann, and L.W. Wilson, Phys. Rev. **C20**, 2267 (1979).
18. S. Pratt, T. Csörgő, and J. Zimányi, Phys. Rev. **C42**, 2646 (1990); S. Pratt, Phys. Rev. **D33**, 72 (1986).
19. H. Bøggild, *et al.* (NA44 Collaboration), Phys. Lett. **B302**, 510, (1993); D. Hardtke, Ph.D. dissertation, The Ohio State University (1997).
20. D.A. Brown and P. Danielewicz, Phys. Lett. **B398**, 252 (1997).
21. T. Csörgő, B. Lörstad, and J. Zimányi, Z. Phys. **C71**, 491 (1996).